Birds breathe at an aerodynamic resonance

Cite as: Chaos **31**, 123132 (2021); https://doi.org/10.1063/5.0069696
Submitted: 01 September 2021 • Accepted: 04 December 2021 • Published Online: 30 December 2021

Facundo Fainstein, Sebastián M. Geli, Ana Amador, et al.

Birds breathe at an aerodynamic resonance

Cite as: Chaos **31**, 123132 (2021); doi: 10.1063/5.0069696
Submitted: 1 September 2021 · Accepted: 4 December 2021 ·
Published Online: 30 December 2021

Facundo Fainstein,[1] Sebastián M. Geli,[1] Ana Amador,[1,2] Franz Goller,[3,4] and Gabriel B. Mindlin[1,2,a)]

AFFILIATIONS

[1]Departamento de Fisica, FCEyN, Universidad de Buenos Aires, Buenos Aires 1428, Argentina
[2]IFIBA, CONICET, Buenos Aires 1428, Argentina
[3]Institute of Zoophysiology, University of Münster, Münster 48143, Germany
[4]School of Biological Sciences, University of Utah, Salt Lake City, Utah 84112, USA

[a)]**Author to whom correspondence should be addressed:** gabo@df.uba.ar

ABSTRACT

We present a dynamical model for the avian respiratory system and report the measurement of its variables in normal breathing canaries (*Serinus canaria*). Fitting the parameters of the model, we are able to show that the birds in our study breathe at an aerodynamic resonance of their respiratory system. For different respiratory regimes, such as singing, where rapid respiratory gestures are used, the nonlinearities of the model lead to a shift in its resonances toward higher frequency values.

At what rate do birds breathe? At what rate do they produce their syllables during singing? Behavior emerges from the interaction of a nervous system, a biomechanical periphery, and the environment. Birds have high metabolic rates and require a continuous supply of oxygen. For that reason, it is not surprising that they developed a highly efficient respiratory system. In this work, we derive a model for the avian respiratory system and discuss how its nonlinearities constrain the emergent behavior. We fit the parameters of the model and show that normal respiration operates at its resonance. For other respiratory regimes, the nonlinearities of the system shift the frequencies at which it operates optimally. More generally, this result is consistent with an emerging picture where several life supporting devices are strikingly fine-tuned to the sources of energy that powers them.

I. INTRODUCTION

The avian respiratory system facilitates high rates of gas exchange and plays an important role in thermoregulation. Birds have relatively small and rigid lungs, which are ventilated by the attached set of nine air sacs framed by a thoraco-abdominal complex.[1] Posterior and anterior air sacs are compressed and expanded simultaneously, and aerodynamic valves contribute to establishing a unidirectional flow of air through the lung.[2,3] The lung is, therefore, perfused with oxygenated air during both respiratory phases.

Airflow during inspiration and expiration is driven by muscle action,[4] which moves a significant mass[5] (the sternum, rib cage, and overlying muscles) and, therefore, either compresses or expands the air sacs. In contrast to mammals, expiration is not driven passively because birds do not utilize a diaphragm muscle to power inspiration. Ventilation is determined by respiratory rate and depth, and the two parameters are controlled by the nervous system. Because respiration constitutes a significant energy expenditure (about 4% of the total metabolism),[6] it is natural to expect that this continuously operated biomechanical device is efficiently operated. It is the purpose of this work to explore to what degree the respiratory rate is attuned to the biomechanics of the avian respiratory system.

The dynamics behind the efficiency of this complex device has been experimentally investigated in the past.[7,8] In those experimental paradigms, anesthetized subjects were artificially ventilated, while aerodynamical variables were measured. In these experiments, the respiratory system displayed resonances at frequency values compatible with panting, a shallow respiratory gesture involved in thermoregulation. However, mechanical interventions were necessary to prevent the syrinx from acting as a flutter valve, raising the question whether the results also apply to an unmanipulated, naturally breathing bird.

In this work, we use data driven techniques in order to estimate the parameters of a dynamical system describing the dynamics of the respiratory system during normal breathing. In particular, we measure the air sac pressure and thoracic wall displacement in awake and normally breathing birds. We develop a simplified biomechanical

model capturing the basic mechanisms of the system's dynamics and fit its parameters with the recorded data. Exploring the resonances of this dynamical system for different subjects, we find that they match the birds' normal respiratory rates. This result is consistent with an emerging pattern where several life supporting devices and mechanisms are strikingly fine-tuned to the sources of energy that powers them.[9,10]

II. RESULTS

A. A simple model for a forced open cavity

The compression and expansion of the sacs is achieved when the thoraco-abdominal complex changes its configuration, driven by inspiratory and expiratory muscles [see Fig. 1(a)].[11,12] During inspiration, all the air sacs expand. The posterior air sacs incorporate air from the exterior and the anterior sacs from the lungs. During expiration, aerodynamic valves prevent the air in the posterior sacs to be expelled back to the atmosphere.[13] Alternatively, it is directed to the lungs. Similarly, during the expiration, aerodynamic valves prevent the air in the anterior sacs to return to the lungs; instead, the flow is directed to the atmosphere. Since both compression and expansion of the sacs occur while one of their valves is open, the relationship between their volume and pressure is dynamical in nature.

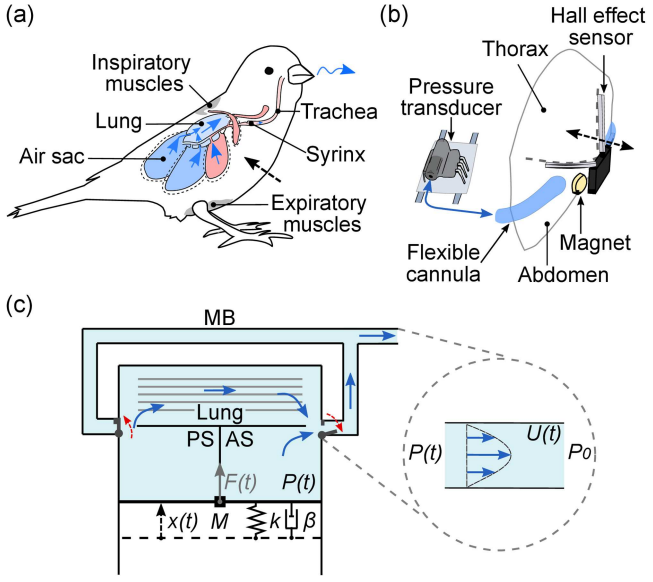

FIG. 1. The avian respiratory system: schematics, physiological measurements, and biomechanical model. The black dashed arrows represent thoracic wall displacement, and the solid blue ones represent airflow. (a) Schematics of the avian respiratory system during expiration, showing the sets of compressed posterior air sacs (PS, blue) and anterior air sacs (AS, red), respiratory muscles, lung, and trachea. (b) The sensors used to measure physiological variables proportional to the mathematical variables of the model. (c) A diagram illustrating the variables of the dynamical model. Red dashed arrows schematize the action of the aerodynamic valves. MB stands for "mesobronchus," and the gray parallel lines inside the lung represent the parabronchi.

To capture the basic dynamics involved in the respiratory system, we develop a dynamical model that can be represented as a single piston of mass M pushing the air in a cylinder with three cavities, as shown in Fig. 1(c). In this model, the piston represents the sternum, the rib cage, and the overlying muscles. The movement of the piston changes the volume of two of the three cavities, representing the anterior and posterior air sacs, while the volume of the cavity representing the lung is not changed. We assume that the pressure in the anterior and posterior sacs is the same, an approximation consistent with Refs. 14 and 15, where it is reported that differential pressures between the sacs during quiet breathing are very small. If $x(t)$ denotes the piston's departure from its equilibrium position, its dynamics can be described using Newton's second law of motion,

$$M\frac{d^2x(t)}{dt^2} = -kx(t) - \beta\frac{dx(t)}{dt} - A(P(t) - P_0) + F(t). \quad (1)$$

On the right side of the equation, the first term accounts for an elastic restitution (k is the restitution constant), the second term for the dissipative losses (β is the dissipative constant), and the third term represents the force due to pressure imbalance between the interior [where the gas in the sacs is at pressure $P(t)$] and exterior (at constant pressure P_0) of the cylinder. The last term accounts for the external forces exerted by the expiratory and inspiratory muscles. Following Ref. 11, during normal breathing, expiratory and inspiratory gestures are approximated by square functions.

Using the equation of state for an ideal gas ($P\,V = Nk_BT$) and writing the volume of the system as $V(t) = V_0 - Ax(t)$ (with V_0 as the equilibrium volume and A as the area of the piston surface), we can relate the pressure variation (dP) with the piston's displacement (dx) and the change of mass in the cylinder (dN). In this way, assuming that the temperature T is constant, we can write the pressure variation as

$$dP = \frac{N(t)k_BT}{(V_0 - Ax(t))^2}Adx + \frac{k_BT}{V_0 - Ax(t)}dN, \quad (2)$$

where

$$dN = -\rho U dt \approx -\rho_0 U dt, \quad (3)$$

with ρ and ρ_0 being the density of air in the interior and exterior, respectively, and U the volume flow. For a laminar flow (the estimated Reynolds number is Re ≈ 500), we can relate the volume flow through an aperture with the pressure difference across it as $U = \alpha\Delta P$, where $\Delta P(t) = P(t) - P_0$. This is consistent with Hartley and Suthers's[16] records in canaries, where α is a parameter whose inverse characterizes the resistance to the airflow.

To represent the existence of two different aerodynamic valves that route the air during inspiration and expiration through different apertures,[13] we can write the flow as

$$U = (\alpha_{ps} - (\alpha_{ps} - \alpha_{as})S(\Delta P))\Delta P(t), \quad (4)$$

with $S(\Delta P) \equiv 1/(1 + e^{-10*\Delta P})$. The sigmoidal function allows us to represent the aperture of different valves at different pressurization states. For a positive pressurization, $S \to 1$ leading to $U \to \alpha_{as}\Delta P$. For negative pressurization, $S \to 0$, and $U \to \alpha_{ps}\Delta P$. This allows us to write a piecewise linear equation to account for the dynamics of

the pressure difference,

$$\frac{d(\Delta P(t))}{dt} = \frac{P_0}{V_0} A \frac{dx(t)}{dt} - \frac{P_0}{V_0} (\alpha_{ps} - (\alpha_{ps} - \alpha_{as}) S(\Delta P)) \Delta P(t). \tag{5}$$

It is interesting to notice that for normal breathing, it is possible to approximate $\alpha_{as} \approx \alpha_{ps} \equiv \alpha$, giving rise to pressure patterns approximately symmetric with respect to the atmospheric pressure.

For quiet breathing and defining $p \equiv \Delta P$, our dynamical system reads

$$\frac{dx}{dt} = y, \tag{6}$$

$$\frac{dy}{dt} = Bx + Cy + Dp + Ef(t), \tag{7}$$

$$\frac{dp}{dt} = Fy + Gp, \tag{8}$$

with

$$(B, C, D, E, F, G) = \left(-\frac{k}{M}, -\frac{\beta}{M}, -\frac{A}{M}, \frac{f_0}{M}, \frac{P_0}{V_0} A, -\frac{P_0}{V_0} \alpha \right), \tag{9}$$

where f_0 is the amplitude of the external forcing. In this approximation, we are neglecting small pressure differences between the air sacs.[14,15] The unidirectionality of the flow is guaranteed by the introduction of the aerodynamic valves, whose apertures are state dependent. Notice that the system can only be written as a forced linear one as long as $\alpha_{as} \approx \alpha_{ps}$, i.e., during quiet breathing. To reproduce other respiratory regimes, we have to explore the solutions of the model outside the realm of this approximation. An analysis of the model in this nonlinear regime is presented in Sec. II D.

B. The measurement of volume and pressure in the sacs

We conducted experiments to measure the air sac pressure and the thoracic wall displacement in three naturally breathing adult male canaries (*Serinus canaria*). Air sac pressure is measured with a flexible silicone cannula inserted into a posterior air sac, with its free end attached to a piezoresistive pressure transducer positioned in a backpack carried by the bird.[16] The thoracic wall displacement is measured with a Hall effect sensor attached to the ribs and a magnet placed under the skin at the abdomen, as shown in Fig. 1(b). As the bird breathes, there is a relative motion between the abdomen and the thorax, which translates into a time dependent magnetic flux density. When the bird inhales, the volume of the air sacs increases, and the thoracic wall supporting the Hall sensor departs from the abdomen. When the bird exhales, the volume decreases and so does the distance between the wall and the abdomen. The presence of the Hall transducer and the magnet was found to not significantly alter the respiratory rate. An extended description of materials and methods is described in the Appendix.

We denote X_r and P_r recorded thoracic wall displacement and air sac pressure. In Fig. 2(a), we show approximately 5 s of simultaneous recordings of both variables. For each one of the three birds in our study, we took several sets of five simultaneous oscillations of X_r and P_r (61 sets from the first bird, 63 from the second one, and 46 from the third bird). We averaged them to obtain a representative oscillation for each set. We denote the representative data $\overline{X_r}$ and $\overline{P_r}$. An example is displayed in Fig. 2(b). For each representative oscillation, we fitted the coefficients of the dynamical system describing our model so that the squared difference between the data and the solutions was minimized[18] (see the Appendix for a detailed description of data analysis). Then, we integrated the model with those parameters and initial conditions from the representative data. A result is displayed with the continuous curves in each panel of Fig. 2(b). The right panel of Fig. 2(b) displays $(\overline{X_r}, \overline{P_r})$ and the solutions of the fitted model (x, p).

C. The fitted dynamical systems present resonances

During quiet breathing, we assume $\alpha_{as} \approx \alpha_{ps}$, and the piecewise linear respiratory model becomes linear. We analyzed the response of the fitted equations to different harmonic components, which can pave the way to explore its solutions when driven by different gestures. For each set of coefficients of the dynamical system obtained from fitting 170 recorded representative oscillations, we explored the solution in the stationary state and plotted the peak-to-peak amplitude of p as a function of the forcing frequency. In Fig. 3, we show the result for each individual. In all the cases, we found curves with a single maximum. The frequency value for which

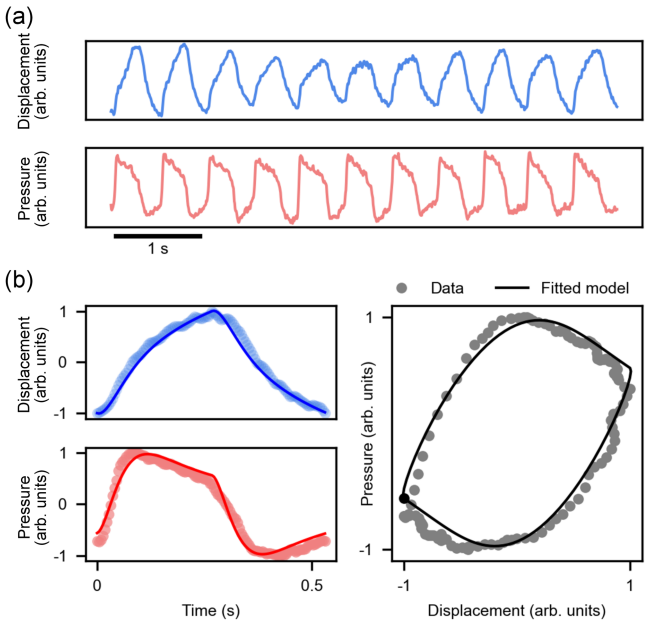

FIG. 2. A simple biomechanical model fits the recorded data. (a) An example of the variables measured in this work: the thoracic wall displacement, whose fluctuations are a proxy for air sac volume changes, and the air sac pressure. Both variables were normalized to the [−1,1] range. (b) Averaging over five consecutive cycles, we obtain a representative oscillation, displayed with dots. The continuous lines show the solutions of our model with parameters minimizing the squared difference between the simulations and the data. The right panel shows the projection of the dynamics in $(\overline{X_r}, \overline{P_r})$ and the integrated variables (x, p).

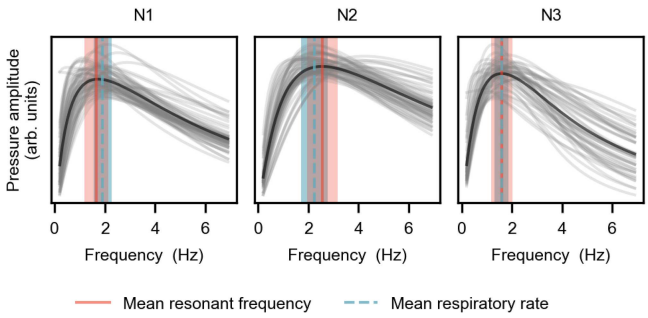

FIG. 3. Frequency response of the fitted dynamical systems (variable p) to harmonic forcing. In gray, we display the responses using the parameters obtained from fitting 170 representative oscillations measured from three different birds (N1, N2, and N3). Black curves represent the average pressure amplitude of the model's solutions for each forcing frequency. Red vertical lines show the mean resonant frequencies and the blue dashed ones the mean respiratory rates. Shaded areas are the intervals around the mean with a two standard deviation width. Resonant frequencies and respiratory rates present overlapping distributions.

the curve displays a maximum is called the resonance frequency. In Fig. 4(a), we show the frequency response using the coefficients that fitted the representative oscillation displayed in Fig. 2(b). We computed 170 resonant frequencies, and their distribution is shown (in red) in Fig. 4(b). In blue, we show the distribution of the average respiratory rates, computed for each of the 170 segments selected for our analysis. In Fig. 4(c), we display the distribution of resonant frequencies and the distribution of respiratory rates, together with the syllabic rates used during song production.[19] The respiratory rates r_{resp} were found to be $r_{\text{resp}} = (1.95 \pm 0.04)$Hz, while the resonant frequencies $\omega_{\text{res}} = (1.97 \pm 0.05)$Hz (mean $\pm$ standard error). The Wilcoxon rank sum test provides a p-value $p_W = 0.8$, suggesting that they come from distributions with the same mean values. Notice that the similarity is remarkable considering the wide range of respiratory gestures that a bird is capable of doing, for example, during birdsong production [see Fig. 4(c)].

Birds also operate their respiratory system in different regimes. For example, during panting, they reduce the airflow resistance by further opening the syringeal valves within the respiratory system. We explored our model for values of the parameter accounting for flow resistance in order to emulate that change and found that the resonant frequencies increase [see Fig. 5(a)]. This is consistent with the characteristic faster respiratory pace of panting.

D. Analysis of the model during birdsong production

In our analysis of quiet respiration, we assumed that $\alpha_{as} \approx \alpha_{ps} \equiv \alpha$. This allows the model to display symmetric solutions for the pressure when driven by symmetric forces. If this condition is not satisfied, the model becomes piecewise linear and reads

$$\frac{dx}{dt} = y, \tag{10}$$

$$\frac{dy}{dt} = Bx + Cy + Dp + Ef(t), \tag{11}$$

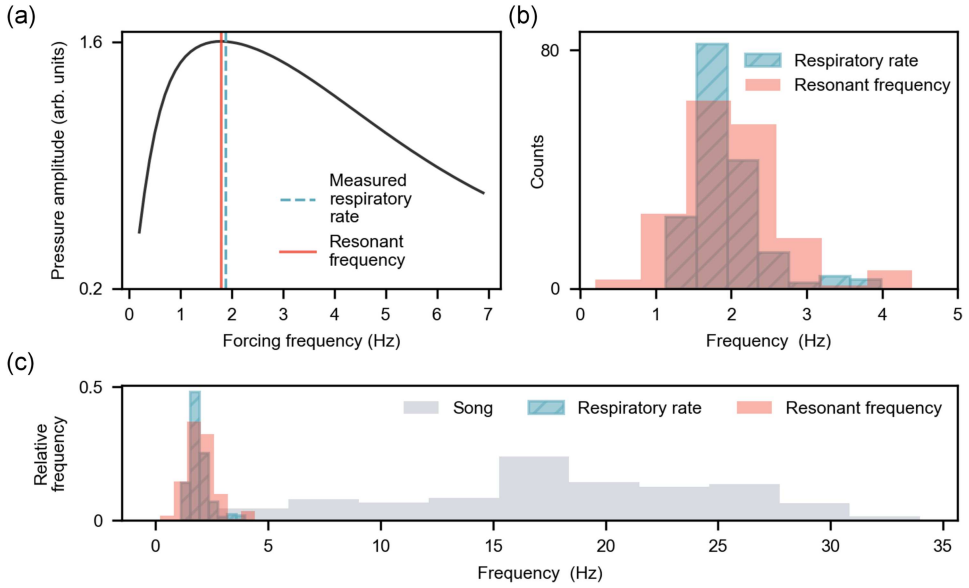

FIG. 4. The fitted dynamical model presents aerodynamic resonances at normal respiratory rates. (a) Frequency response of the dynamical system (variable p) to harmonic forcing, with its parameters adjusted so that its solutions fit the recordings in Fig. 2(b). The frequency at which the response is maximum is the resonant frequency (red solid line). The blue dashed line shows the average respiratory rate computed from the five consecutive oscillations used in this example. (b) The procedure is repeated for 170 sets of five cycles each, measured from three different birds. The distribution of the resonant frequencies in red and the respiratory rates in blue. (c) The histograms are shown together with the syllabic rates computed from singing respiratory gestures of the three birds in our study.

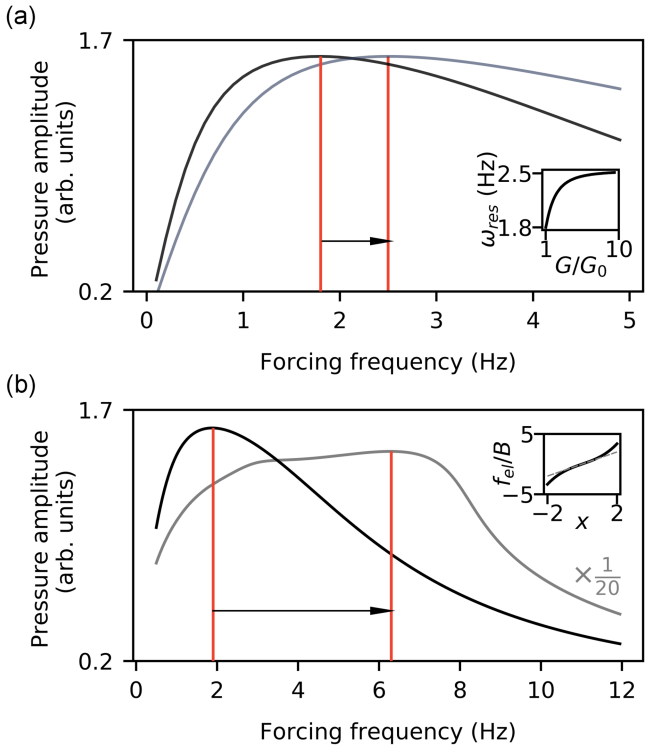

FIG. 5. The model gives rise to a shift of the resonance when parameters are varied to emulate some features present in other respiratory regimes. The y axis shows the pressure peak-to-peak amplitude in the stationary state. The frequency response of the normal breathing fitted dynamical system is showed in black lines, and the coefficients of the model simulation displayed in Fig. 2(b) are used. (a) A joint decrease in flow resistance for expiration and inspiration, as expected to occur during panting, leads to an increase in the resonant frequency. In gray line, we show the frequency response when $G = 9G_0$, where G_0 is the coefficient of Fig. 2(b). The inset displays the resonant frequency as a function of the relative increment in the coefficient G. (b) The inset shows the non-linear elastic force per unit mass, in a black line, and the linear approximation, in a gray dashed line. Both variables are in arbitrary units. During song, an increase (decrease) in flow resistance during expiration (inspiration) and a larger forcing is expected. This produces a shift in the resonance of the model (gray line). Song like frequency response is divided by 20 for clarity in the comparison. To emulate song, G_{as} and G_{ps} are chosen so that pressure expiratory gestures represent 80% of peak to peak amplitude when driven by a harmonic function of 10 Hz. For that forcing, the coefficient E is chosen so that pressure and displacement amplitude increase 10 and 3 fold normal breathing amplitude, respectively. The coefficients used are $(B, C, D, E, F, G_{ps}, G_{as}, \varepsilon) = (-254, -41.6, -152, 14\,300, 1.96, -51.1, -4.26, 0.170)$.

$$\frac{dp}{dt} = Fy + (G_{ps} - (G_{ps} - G_{as})S(\Delta P))p, \tag{12}$$

where $G_{as} = -\frac{P_0}{V_0}\alpha_{as}$ and $G_{ps} = -\frac{P_0}{V_0}\alpha_{ps}$. The integration of our model for $G_{as} \neq G_{ps}$ leads to non-symmetric solutions, which is convenient to reproduce other respiratory regimes.

When a bird sings, the syringeal labia are actively pushed together, which increases the resistance to airflow during expiration. This is translated into our model by assuming that $|G_{as}| < |G_{ps}|$

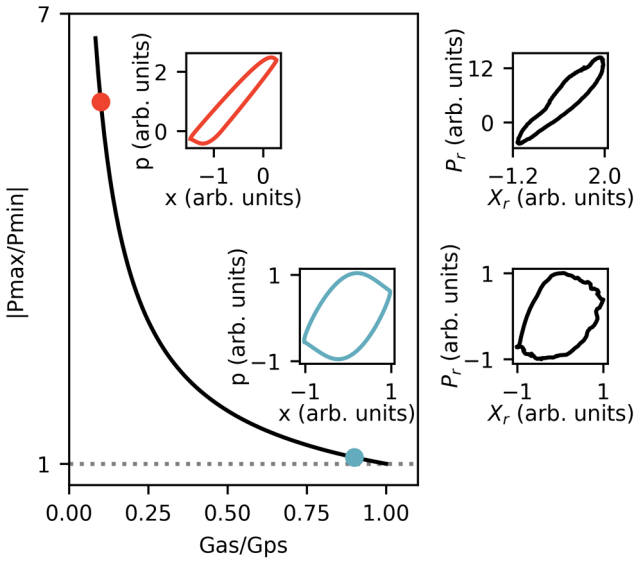

FIG. 6. An increase of flow resistance during expiration leads to a regime where pressure expiratory gestures are larger than inspiratory ones, as observed during birdsong production. The y axis is the ratio of pressure maximum and minimum absolute values. The x axis is the ratio of the expiratory and inspiratory G value. The parameters and forcing function used for this plot were the ones fitted to the recordings in Fig. 2(b), where G_{ps} was fixed to its original value and only G_{as} was varied. The right panels show experimental recordings of displacement and pressure during normal respiration (lower) and song (upper). Note that the phase difference between simulated pressure and displacement decreases when expiratory resistance is increased, as observed in measurements during song.

since the inverse of $|G|$ is proportional to the flow resistance. A measure of the asymmetry of the pressure solutions when G_{as}/G_{ps} is varied between (0, 1) is displayed in Fig. 6. The simulations are consistent with the data, which show that, typically, pressure expiratory gestures are larger than inspiratory ones during singing. Moreover, an increase in the expiratory resistance leads to a decrease in the phase difference between pressure and displacement, which is also observed in the data (see Fig. 6). Besides these considerations, respiration during song involves a larger forcing.[11,12] It has been reported that, for larger values of volume change, the magnitude of the elastic force increases significatively, departing from the linear approximation.[17]

To reproduce this experimental result, we introduce a cubic elastic force per unit mass,

$$f_{el}(x) = B\,(1 + \varepsilon x^2)\,x. \tag{13}$$

We estimate that the elastic restitution, defined as the slope of the elastic force, duplicates when the displacement increases by a factor of two of normal breathing amplitude.[17] This implies $\varepsilon = 0.17$ (arb. units).

We explored the resonances of the model when this nonlinear effect is included and found that resonant frequencies increase [see Fig. 5(b)].

III. DISCUSSION

It is natural to expect breathing, a behavior active at every moment of an animal's life, to be fine-tuned to its source of energy. In this work, we presented a simple physical model with the main dynamical elements found in an avian respiratory system and fitted its parameters so that its solutions match recorded air sac pressure and a variable describing air sac volume during quiet breathing. We found that this model displays resonances for the pressure at precisely the respiratory rates. This guarantees maximum airflow circulation through the lungs for a given forcing amplitude. The search for optimal respiratory regimes given biomechanical constraints has a rich history, which can be tracked to the study of how the motion of abdominal contents in running mammals could facilitate breathing.[20,21]

Previous studies in birds consisted of direct experimental explorations of preparations that included the use of anesthesia as well as mechanical devices, such as stainless-steel sleeves, for maintaining a certain degree of aperture of the respiratory system. These studies found resonances of the thoraco-abdominal system at panting frequency values. It is likely that the muscle tonicity of the anesthetized animal as well as the non-natural aperture of the respiratory system used in the preparation might alter the resonances of the respiratory system. In this work, we revisited the problem by fitting the parameters of a biomechanical model with simultaneously recorded variables describing the state of the biomechanical device controlling respiration in spontaneously breathing birds with unmanipulated respiratory tracts. For the group data from the three birds analyzed, the resonant frequencies and the respiratory rates displayed similar distributions. We could successfully fit a model assuming similar parameters for the expiratory and inspiratory cycles. During singing, this approximation will not hold. Vocalization requires different input and output flow resistances as well as the use of stronger forcing. This leads to a regime where the system is stiffer, shifting the resonances toward higher values. Suggestively, for the species analyzed in this work, the syllabic rate during birdsong production is higher than the quiet respiratory rate.

From metabolic cycles to self-replication, fine tuning of the system's performance to the source of energy appears as a generic physical feature of life. Our results, which indicate that maximal air flow is guaranteed to occur at normal breathing rates, are an example of this principle at the macroscopic scale.

ACKNOWLEDGMENTS

We acknowledge partial financial support from the ANPCyT-FONCyT (Argentina) under Grant No. PICT-2018-00619.

AUTHOR DECLARATIONS

Conflict of Interest

The authors declare that there is no conflict of interest.

Ethics Approval

The experiments were conducted following the protocols of the CICUAL (committee for care and use of animals in the laboratory) of the School of Sciences of the Universidad de Buenos Aires (c.n.113).

DATA AVAILABILITY

All raw recorded respiratory data, the codes used for the analyses and for generating the figures as well as the coefficients obtained from the fitting procedure presented in this paper are openly available in Zenodo at https://doi.org/10.5281/zenodo.4897939, Ref. 22.

APPENDIX: MATERIALS AND METHODS

The air sac pressure P_r was measured inserting a flexible silicone cannula (AM-systems Silicone Tubing $0.030'' \times 0.065'' \times 0.0175''$ Catalog No. 807000) right below the last rib, 5 mm into the posterior air sac. The free end is attached to a piezoresistive pressure transducer (FHM-07 PGR from Fujikura), positioned in a backpack carried by the bird. The variable x is proportional to the magnetic flux density detected by a Hall effect sensor (Hall Effect Sensor ICs A1325 Allegro Microsystems, Inc.) attached to the ribs and the sternum, which is generated by a magnet placed under the skin at the abdomen. To test if the presence of the Hall transducer altered the respiratory dynamics, we compared the respiratory rate of the three individuals reported in this study, with the distribution of respiratory rates obtained from 316 respiratory cycles of six other individuals. The mean respiratory rate of the individuals in our study, in which air sac pressure and thoracic wall displacement were measured, was (1.95 ± 0.04) Hz. The mean respiratory rate of six other individuals in which only air sac pressure was measured was found to be (1.94 ± 0.02) Hz.

For the three birds in our study, we took several sets of five oscillations and for each set computed a representative oscillation as follows. For each set i, we computed the number of points between the five consecutive minima and maxima of the recorded thoracic wall displacement X_r $(k^{i,j}_{up}, \quad j = 1, \ldots, 5)$ and the number of points between the five consecutive maxima and minima of X_r $(k^{i,j}_{\text{down}}, \quad j = 1, \ldots, 5)$. Then, we computed the average number of points $\left\langle k^i_{\text{up}} \right\rangle$ and $\langle k^i_{\text{down}} \rangle$ and resampled the data using linear interpolations so that every segment of time trace between consecutive minima and maxima of the ith set has $\left\langle k^i_{\text{up}} \right\rangle$ points, and every segment of time trace between consecutive maxima and minima of the ith set has $\langle k^i_{\text{down}} \rangle$ points. For each set i, we averaged the five segments between consecutive minima and maxima, as well as the five segments between consecutive maxima and minima. In this way, we computed a representative oscillation for the ith set. The time series of the variable P_r was resampled using the same time steps followed to process the X_r time series.

The parameters B, C, D, E, F, and G in the dynamical system, Eqs. (6)–(8), were fitted after assuming $f(t)$ to be a square function of time, equal to the sign function of the slope of X_r. This assumption is consistent with the measurements displayed in Ref. 11 and allows reproducing the sharp changes in the slope observed in the time traces of the pressure. For each

representative oscillation (obtained as the average over five consecutive cycles), we performed 25 random choices of initial coefficients within the following ranges: $B, C, D, G \in (-5000, 0)$, $E, F \in (0, 5000)$. For each choice, we carried out a Nelder–Mead fit to minimize the squared difference between the data and the integrated model (χ^2). The library lmfit implemented for Python was used.[18] The optimal parameters were the ones that minimized χ^2 within the 25 fits. For the case illustrated in Fig. 2(b), $(B, C, D, E, F, G) = (-254, -41.6, -152, 476, 1.96, -17.0)$, leading to a reduced chi-squared: $\chi^2_\nu = \chi^2/N - \upsilon = 0.013$. This procedure was repeated for 170 segments of data, obtaining $(\mu_{\text{respiration}}, \sigma_{\text{respiration}}) = (1.95\,\text{Hz}, 0.49\,\text{Hz})$ and $(\mu_{\text{resonance}}, \sigma_{\text{resonance}}) = (1.97\,\text{Hz}, 0.69\,\text{Hz})$.

REFERENCES

[1] H. R. Duncker, "The lung air sac system of birds. A contribution to the functional anatomy of the respiratory apparatus," Ergeb. Anat. Entwicklungsgesch **45**, 7–171 (1971).
[2] C. G. Farmer, "Pulmonary transformations of vertebrates," in *The Biology of the Avian Respiratory System*, edited by J. N. Maina (Springer, 2017), pp. 99–112.
[3] Q. M. Nguyen *et al.*, "Flow rectification in loopy network models of bird lungs," Phys. Rev. Lett. **126**, 114501 (2021).
[4] L. P. Claessens, "The skeletal kinematics of lung ventilation in three basal bird taxa (emu, tinamou, and guinea fowl)," J. Exp. Zool. Part A **311A**, 586–599 (2009).
[5] J. J. Baumel, J. A. Wilson, and D. R. Bergren, "The ventilatory movements of the avian pelvis and tail: Function of the muscles of the tail region of the pigeon (*Columba livia*)," J. Exp. Biol. **151**, 263–277 (1990).
[6] J. S. Markley and D. R. Carrier, "The cost of ventilation in birds measured via unidirectional artificial ventilation," Comp. Biochem. Physiol. Part A **155**, 146–153 (2010).
[7] G. Kampe and E. C. Crawford, Jr., "Oscillatory mechanics of the respiratory system of pigeons," Respir. Physiol. **18**, 188–193 (1973).
[8] E. C. Crawford, Jr. and G. Kampe, "Resonant panting in pigeons," Comp. Biochem. Physiol. Part A **40**, 549–552 (1971).
[9] J. L. England, *Every Life Is on Fire: How Thermodynamics Explains the Origins of Life* (Basic Books, 2020).
[10] J. L. England, "Dissipative adaptation in driven self-assembly," Nat. Nanotechnol. **10**, 919–923 (2015).
[11] R. S. Hartley, "Expiratory muscle activity during song production in the canary," Respir. Physiol. **81**, 177–187 (1990).
[12] J. M. Wild, F. Goller, and R. A. Suthers, "Inspiratory muscle activity during bird song," J. Neurobiol. **36**, 441–453 (1998).
[13] J. P. Butler, R. B. Banzett, and J. J. Fredberg, "Inspiratory valving in avian bronchi: Aerodynamic considerations," Respir. Physiol. **72**, 241–255 (1988).
[14] D. F. Boggs, P. J. Butler, and S. E. Wallace, "Differential air sac pressures in diving tufted ducks *Aythya fuligula*," J. Exp. Biol. **201**, 2665–2668 (1998).
[15] J. H. Brackenbury, "Lung-air-sac anatomy and respiratory pressures in the bird," J. Exp. Biol. **57**, 543–550 (1972).
[16] R. S. Hartley and R. A. Suthers, "Airflow and pressure during canary song: Direct evidence for mini-breaths," J. Comp. Physiol. A **165**, 15–26 (1989).
[17] J. Scheid and J. Piiper, "Volume, ventilation and compliance of the respiratory system in the domestic fowl," Respir. Physiol. **6**, 298–308 (1969).
[18] M. Newville, T. Stensitzki, D. B. Allen, and A. Ingargiola, "lmfit: Non-linear least-square minimization and curve-fitting for Python," Zenodo, version 1.0.1 (May 7, 2020), http://doi.org/10.5281/zenodo.3814709
[19] L. M. Alonso, J. A. Alliende, F. Goller, and G. B. Mindlin, "Low-dimensional dynamical model for the diversity of pressure patterns used in canary song," Phys. Rev. E **79**, 041929 (2009).
[20] D. M. Bramble and D. R. Carrier, "Running and breathing in mammals," Science **219**(4582), 251–256 (1983).
[21] D. M. Bramble, "Biomechanical and neuromotor factors in mammalian locomotor-respiratory coupling," in *Nonlinear Oscillations in Biology and Chemistry*, edited by H. G. Othmer (Springer, Berlin, 1986), pp. 130–149.
[22] F. Fainstein, S. M. Geli, A. Amador, F. Goller, and G. B. Mindlin (2021). "Data and code for 'Birds breathe at an aerodynamic resonance,'" Zenodo. http://doi.org/10.5281/zenodo.4897939